Enhanced Coupled Mechanical-Acoustic Field Computations on Nonmatching Grids

Simon Triebenbacher[a], Manfred Kaltenbacher[a], Martin Meiler[b] and Hermann Landes[b]

[a]Univ. Erlangen-Nuremberg, Dept. of Sensor Technology, Paul-Gordan-Str. 3/5, 91052 Erlangen, Germany
[b]Simetris GmbH, Am Weichselgarten 7, 91058 Erlangen, Germany
simon.triebenbacher@lse.eei.uni–erlangen.de

In this work we extend our research on nonmatching finite element grids, as used in the analysis of coupled mechanical-acoustic systems, from standard (bi-)linear grids to higher order Lagrangian grids. In practical applications, like the simulation of thin membranes or the computation of the acoustic field in a large homogeneous domain, the use of higher order finite elements is often advantageous. To demonstrate the practical applicability we investigate the computation of electrodynamic loudspeakers.

To keep the number of unknowns as low as possible the discretization should be chosen as coarse as possible without becoming susceptible to numerical dispersion. Due to the same reason it is also desirable to use a uniform discretization and to be able to adjust the approximation order.

To gain more flexibility, we introduce a nonmatching interface between the subdomains and discretize them independently, both in space and approximation order. Our enhanced scheme applies the mortar finite element method to coupled mechanical-acoustic field problems.

1 Introduction

In the present paper we conduct numerical studies concerning the practical applicability of the mortar FEM for mechanical-acoustic coupling in an electrodynamic loudspeaker.

Electrodynamic loudspeakers like the one depicted in Fig. 1 can be encountered in many everyday devices. Among others one should especially mention HiFi systems for home entertainment or cars. Manufacturers of such systems face the challenge to design their actuators, e.g. according to changing geometries or material properties, in the interior of cars. To avoid the costly process of building prototypes, conducting measurements and redesigning, the use of CAE tools is of major importance for the reduction of costs during the development phase of a new product.
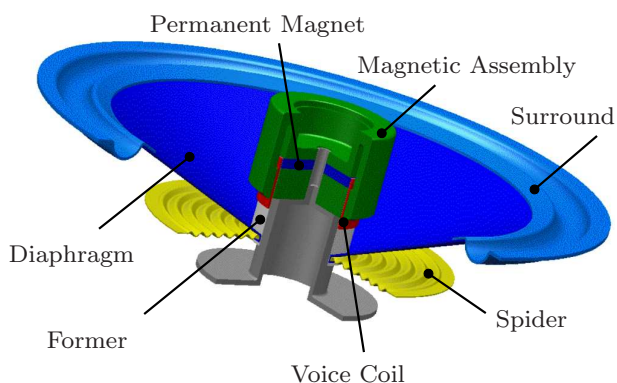

Figure 1: Schematic of an electro-dynamic loudspeaker

In a previous work [6] at our department a complete CAE workplace for the design of electrodynamic loudspeakers has been developed. The standard FEM has been used to model the linear and nonlinear interaction of electromagnetic, mechanical and acoustical fields for small signal and large signal analyses.

In this work we restrict ourselves to the study of the small signal behavior of the elasto-acoustic coupling and show that by applying the mortar FEM, we can further improve the methods developed in [6]. Since the mechanical parts of a loudspeaker need much finer spatial discretization than the acoustic propagation domain, we gain a lot of modelling flexibility, because we are not restricted to geometrically conforming triangulations of the problem domain anymore. Due to the same reason we can choose a very uniform and quite coarse grid for acoustics. In each sub-domain we are able to choose the approximation order independently. Increasing the ap-

proximation order in acoustic sub-domains is justified by the fact that the solution is known to be very smooth, and that we can reduce numerical dispersion [1]. For mechanics this reduces locking effects.

The current paper is organized into the following sections: In section 2 we give a brief introduction to the mortar FEM in the context of mechanical-acoustic and acoustics-acoustics coupling. In section 3 we describe the geometrical setup of the loudspeaker as well as the types of analyses we perform and the applied loads and boundary conditions. Section 4 presents the results of our calculations. We draw a conclusion in section 5 and give an outlook to future studies.

2 Mortar Finite Elements

The term "mortar finite elements" refers to the fact that in this extension to the standard FEM different discretizations, which can be nonmatching in general may be used in the geometrical subdomains of a problem (cf. Fig. 2). The sub-domains get "glued" together by a special formulation.
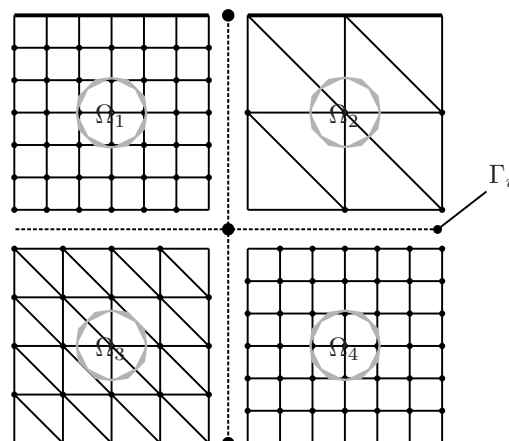

Figure 2: Example for a nonmatching grid with four sub-domains $\Omega_{i=1...4}$ and internal interfaces $\Gamma_{i=1...4}$

This method has several advantages:

- Independent discretizations in sub-domains allows tuning of the element size for each physical field in multiphysics problems.

- Approximation order can be chosen independently for each sub-domain.

- Preprocessing is much more flexible since grids in different sub-domains do not influence each other.

- The method can be used for parallelization. If only a single physical field is involved, our method can be classified as a Finite Element Tearing and Interconnection dual-primal (FETI-DP) method in domain decomposition terms (see e.g. [2])

In this section we introduce the extended formulations for linear mechanical-acoustic and acoustics-acoustics couplings. The generic geometrical setup can be seen in Fig. 3.
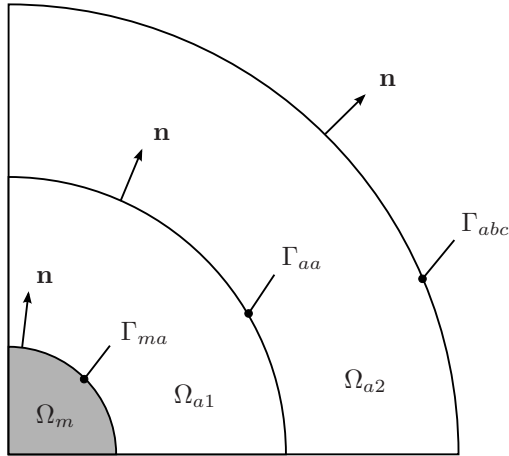

Figure 3: Generic geometrical setup for elasto-acoustic and acoustic-acoustic couplings

We use the standard linear wave equation for acoustics written in pressure formulation with c being the speed of sound

$$\mathbf{\Delta} p = \frac{1}{c^2}\frac{\partial^2 p}{\partial t^2} \quad \text{on} \quad \Omega_{a1,a2} \ . \tag{1}$$

We use the linear PDE for mechanics with the differential operator $\mathcal{B}$, elasticity tensor $[\mathbf{c}]$, volume forces $\mathbf{f}_V$ and density ρ_m

$$\mathcal{B}^{\mathrm{T}}[\mathbf{c}]\mathcal{B}\mathbf{u} + \mathbf{f}_V = \rho_m \frac{\partial^2 \mathbf{u}}{\partial t^2} \quad \text{on} \quad \Omega_m \ . \tag{2}$$

To simulate free field radiation at the boundary of our computational domain we apply the standard absorbing boundary condition (cf. [5])

$$\left(\frac{\partial}{\partial t} + c\frac{\partial}{\partial \mathbf{n}}\right) p = 0 \quad \text{on} \quad \Gamma_{abc} \ . \tag{3}$$

2.1 Mechanical-Acoustic Coupling

At the interface Γ_{ma} between the mechanical and the first acoustic sub-domain we require that the mechanical surface normal velocity $\mathbf{v}$ and the acoustic normal particle velocity $\mathbf{v}_a$ be equal

$$\mathbf{v} \cdot \mathbf{n} = \mathbf{v}_a \cdot \mathbf{n} \ .$$

In primal field variables this condition can be rewritten as

$$\frac{\partial^2 \mathbf{u}}{\partial t^2} \cdot \mathbf{n} = -\frac{1}{\rho_a} \mathbf{\nabla} p \cdot \mathbf{n} \ , \tag{4}$$

with ρ_a being the density of the acoustic fluid.

Further on we stipulate that the mechanical normal stress acting on the interface is equal to the total acoustic pressure p

$$[\boldsymbol{\sigma}] \cdot \mathbf{n} = -\mathbf{n}p \ . \tag{5}$$

By deriving the weak form of Eq. (1) and substituting Eq. (4) for the arising surface integral we arrive at

$$\sum_{i=1}^{2}\left(\int\limits_{\Omega_{ai}} \frac{1}{c^2} w\ddot{p} \ \mathrm{d}\Omega \quad + \quad \int\limits_{\Omega_{ai}} \mathbf{\nabla} w \cdot \mathbf{\nabla} p \ \mathrm{d}\Omega\right)$$
$$+ \int\limits_{\Gamma_{ma}} \rho_a w \, \mathbf{n} \cdot \ddot{\mathbf{u}} \ \mathrm{d}\Gamma = 0 \ . \tag{6}$$

By using Eq. (5) we obtain for the weak formulation of the mechanical PDE Eq. (2) the following relation

$$\int\limits_{\Omega_m} \rho_m \mathbf{w} \cdot \ddot{\mathbf{u}} \ \mathrm{d}\Omega + \int\limits_{\Omega_m} (\mathcal{B}\mathbf{w})^{\mathrm{T}}[\mathbf{c}]\mathcal{B}\mathbf{u} \ \mathrm{d}\Omega +$$
$$\int\limits_{\Gamma_{ma}} \mathbf{w} \cdot \mathbf{n}p \ \mathrm{d}\Gamma = \int\limits_{\Omega_m} \mathbf{w} \cdot \mathbf{f}_V \ \mathrm{d}\Omega \ . \tag{7}$$

A more detailed derivation can be found in [4] respectively [3].

2.2 Acoustic-Acoustic Coupling

Between two acoustic sub-domains the acoustic pressure and its normal derivative should be continuous in a strong sense, i.e.

$$p_1 = p_1 \quad \text{and} \quad \frac{\partial p_1}{\partial \mathbf{n}} = \frac{\partial p_2}{\partial \mathbf{n}} \quad \text{on} \quad \Gamma_{aa} \ .$$

Since this requirement cannot be fulfilled on an interface with geometrically nonmatching triangulations on both sides, the flux continuity condition will be enforced by introducing a Lagrange multiplier

$$\lambda = -\frac{\partial p_1}{\partial \mathbf{n}} = -\frac{\partial p_2}{\partial \mathbf{n}} \ . \tag{8}$$

The continuity in the trace will be enforced in a weak sense

$$\int\limits_{\Gamma_{aa}} (p_1 - p_2)\,\mu \ \mathrm{d}\Gamma = 0 \ , \tag{9}$$

for all test functions μ out of a suitable Lagrange multiplier space Λ.

After deriving the weak form of Eq. (1) and inserting conditions Eq. (8) and Eq. (9), one arrives at the dual-primal problem

$$\sum_{i=1}^{2}\left(\int\limits_{\Omega_{ai}} \frac{1}{c^2} w_i p_i \ \mathrm{d}\Omega \quad + \quad \int\limits_{\Omega_{ai}} \mathbf{\nabla} w_i \cdot \mathbf{\nabla} p_i \ \mathrm{d}\Omega\right) \tag{10}$$
$$+ \int\limits_{\Gamma_{aa}} (w_1 - w_2)\,\lambda \ \mathrm{d}\Gamma = 0$$
$$\int\limits_{\Gamma_{aa}} (p_1 - p_2)\,\mu \ \mathrm{d}\Gamma = 0 \ .$$

We note that the functions from the Lagrange multiplier space Λ are used as a basis for describing the conormal derivative of p in Eq. (8) and as test function μ to satisfy condition Eq. (9).Since the interface Γ_{aa} is only artificial in our case, i.e. no change in material parameters occurs, we may arbitrarily define one side of the interface as slave or non-mortar side and the other one as master or mortar side. In our work we use the trace space of the triangulation on the non-mortar or slave side as a basis for Λ. For other choices of bases for Λ see [3]. We note that the Lagrange multiplier has to be modified at the crosspoint CP. Details about the implementation of this method can be found in [7].

Finally we apply a standard implicit Newmark time stepping scheme for transient simulations (refer to [5]).

3   Problem Setup

We use our method for the prediction of sound fields of an electro-dynamic loudspeaker under small signal excitation, i.e. all calculations are conducted linear. The geometry and material parameters for a subwoofer with a specified frequency range of 20Hz - 5kHz have been taken from [6]. We restrict our analysis however to the interaction of the mechanical parts with the surrounding air and do not regard themagneto-dynamic-mechanical interaction. The mechanical parts of the loudspeaker, denoted by Ω_m in the following, excluding the magnetic assembly, can be seen in Fig. 4.
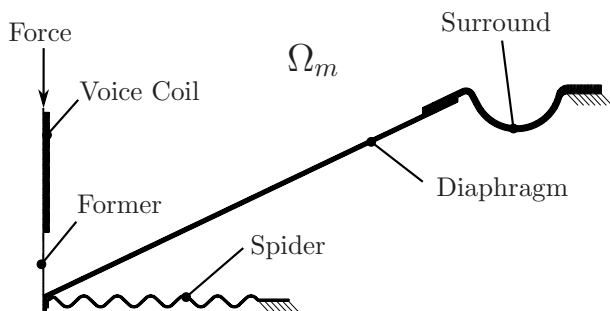

Figure 4: Mechanical parts of loudspeaker.

Our problem domain is axi-symmetric and contains the loudspeaker as well as two acoustic sub-domains. One for the acoustic near field Ω_{a1} and another one for the far field Ω_{a2} as depicted in Fig. 5. The mechanical load gets applied to the former as a pressure load on the top area of former. Its value was chosen to produce relastic sound pressure levels at the point of interest. The assembly is mechanically fixed in both directions at the spider and the surround (cf. Fig. 4).

To demonstrate the flexibility of the method, we compare a number of test cases using harmonic and transient analyses. The reference of all our calculations is a conforming triangulation of the problem domain with standard second order quadrilateral elements as depicted in Fig. 6 taken from [6]. It is important to note that the fine discretization of Ω_m in (CG) affects all other parts of the grid.

For the nonmatching mechanical-acoustic and mechanical-acoustic-acoustic couplings we replace the discretizations of Ω_{a1} and Ω_{a2} with a mixture of triangles and
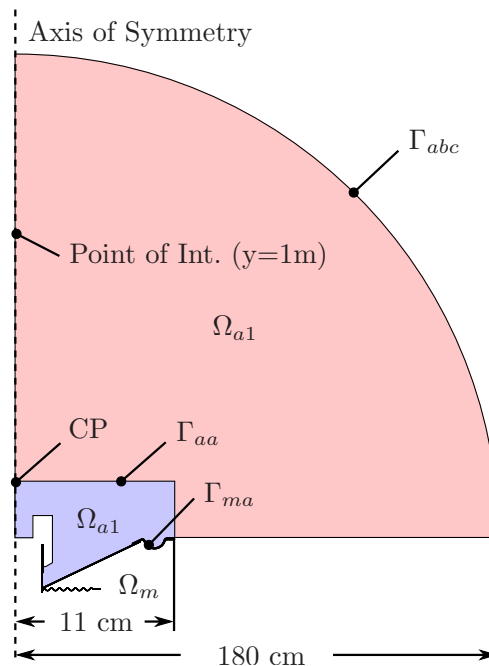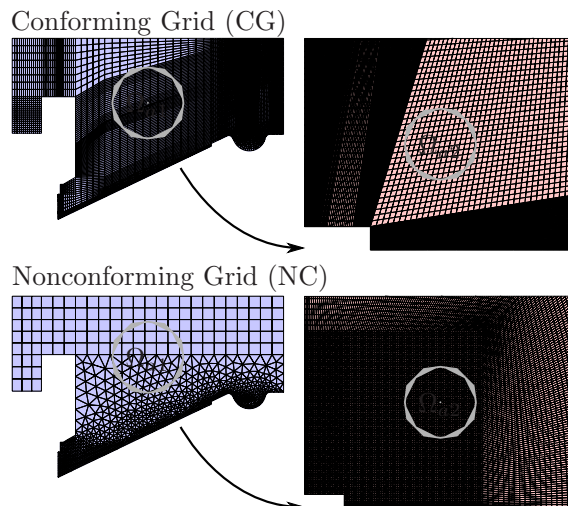

Figure 5: Computational domain.

Figure 6: Overall grid can be composed of several subgrids.

quadrilaterals of different approximation orders. In the latter case an artificial non-matching interface is introduced on Γ_{aa}. For the nonmatching acoustic-acoustic coupling just the discretization of Ω_{a2} is replaced. Table 1 gives an overview of the different setups. The vertical line in each row of the table represents the location of a nonmatching interface. Bold font represents a part of the conforming grid and italic font represents a part of the nonconforming grid.

The maximal element size ($\sim$ 1cm) is chosen to adequately support a frequency (corresponding to the smallest wave-length) of up to 5kHz for linear approximation order. To determine the eigenfrequencies and natural modes of the mechanical system an eigenfrequency analysis is conducted for Ω_m. Further on the resulting signals at the point of interest of coupled mechanical-acoustic transient and harmonic analyses get compared to each other for the frequency range 20Hz - 5kHz. For the transient simulations we use triangle pulse of length

Table 1: Overview of Test Setups

Test case	Ω_m	Ω_{a1}	Ω_{a2}
conforming	**quadr.**		
acou-acou1	**lin.**		*quadr.*
acou-acou2	**quadr.**		*quadr.*
mech-acou1	**lin.**	*quadr.*	
mech-acou2	**quadr.**	*quadr.*	
mech-acou-acou	**quadr.**	*quadr.*	*quadr.*

$T = 60\,\mu s$ as excitation and a timestep of $\Delta t = 5\,\mu s$. Mechanical Rayleigh damping is applied with a loss factor $\tan\delta = 0.25$ for the surround and $\tan\delta = 0.05$ for the other mechanical parts.

4 Numerical Results

4.1 Eigenfrequency analysis

For getting a better understanding about how sound is generated by our experimental setup we conduct a mechanical eigenfrequency simulation on Ω_m with linear and second order approximation. The resulting eigenfrequencies and their corresponding natural modes are shown in Fig. 7

47.41 Hz   353.37 Hz

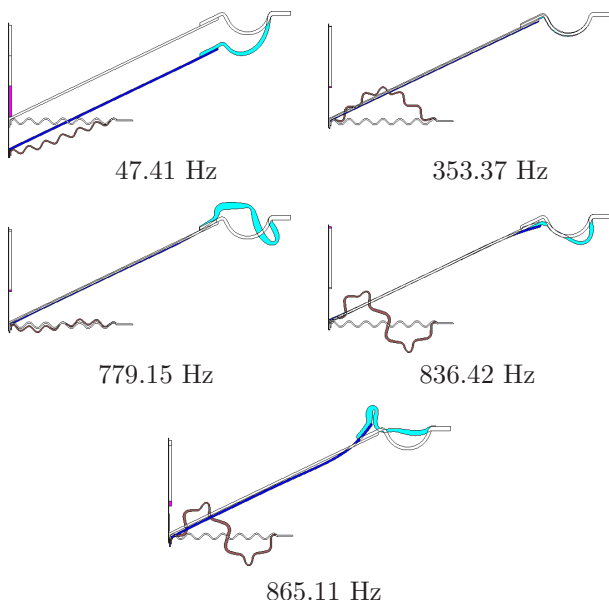779.15 Hz   836.42 Hz

865.11 Hz

Figure 7: Mechanical natural modes of loudspeaker (quadratic).

We can see that the first eigenfrequency is a pure mode of the surround. It is the only mode which considerably contributes to the displacement of the diaphragm. The next mode can be solely attributed to the spider. As frequency gets higher more and more mixed modes are introduced. Their contribution to the displacement

of the diaphragm however, is getting more and more negligible.

Table 2: Eigenfrequencies for lin. and quadr. elements.

linear	quadratic
50.36 Hz	47.41 Hz
366.14 Hz	353.37 Hz
872.99 Hz	779.15 Hz
886.18 Hz	836.42 Hz
1020.78 Hz	865.11 Hz

4.2 Harmonic analysis

For the harmonic analysis we performed a logarithmic frequency sweep in the range of 20Hz - 5kHz. In Fig. 8 we plotted all acoustic pressure amplitude signals at the point of interest. It can clearly be seen, that all of our test setups nearly produce the same results. One can also see, that the lower previously computed mechanical eigenfrequencies are also present in the acoustic signal. The only noticable difference shows up for acou-acou1 and mech-acou1 since the mechanical sub-domain for these cases has been calculated with linear elements. The model is more stiff for these cases therefore the eigenfrequencies move upwards. In Fig. 9 the acoustic pressure field is shown at 5kHz. The detail shows the nonmatching grids in the vicinity of the surround.
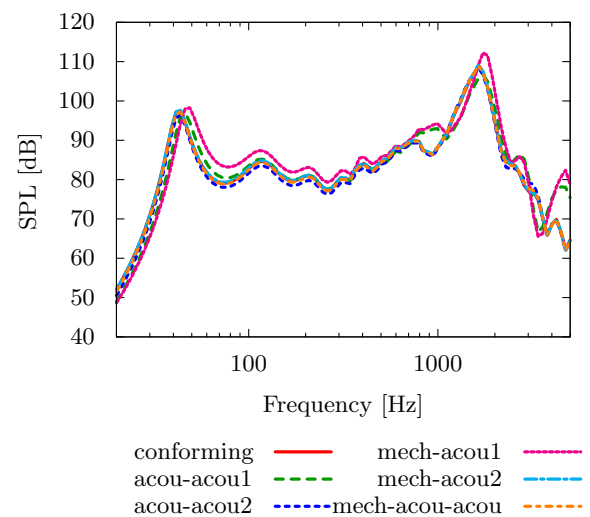

Figure 8: Results of harmonic simulation.

4.3 Transient analysis

The conditions for the spatial discretization when conducting the transient analysis are more demanding compared to the harmonic setting. Since we simulate an exitation by a Dirac pulse which, when transformed into
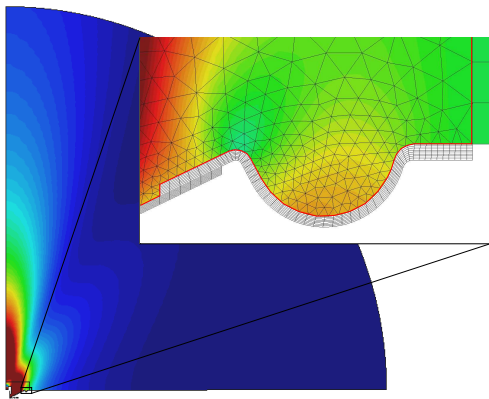
Figure 9: Sound pressure amplitude field at 5kHz (mech-acou-acou).

Figure 11: Transient sound pressure field at $t = 4\,ms$ (mech-acou2).

the frequency domain, contains a broad range of frequencies, spurious reflections may be generated especially at acoustic-acoustic interfaces. Our spatial discretization is tuned however for a maximum frequency of 5kHz, but the excitation signal may contain even higher frequencies than that which the discretizations on both sides can not handle appropriately. Nonetheless our method works well for all test cases as Fig. 10 shows. In Fig. 11 the pressure pulse is depicted shortly after passing the point of interest.
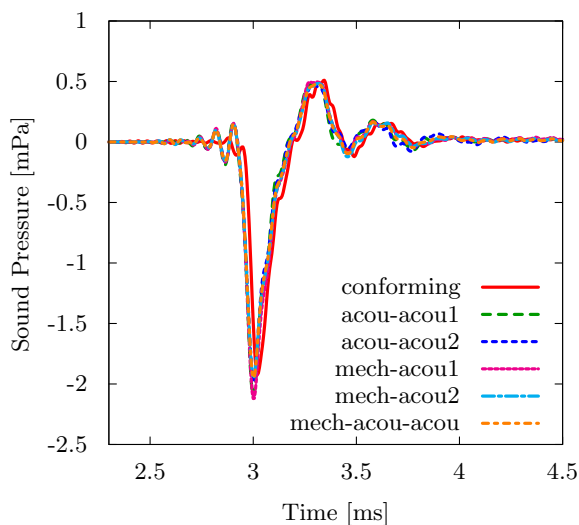

Figure 10: Results of transient simulation.

5   Conclusion

We have shown that by using the mortar FEM great benefits arise for the analysis of mechanical-acoustic coupled problems. The method greatly improves modelling flexibility since grids in subdomains may be completely independent from each other. This is not only true for the spatial discretization but also for the order of approximation. The method is suited for conducting harmonic and transient analyses. If required, the method can also be used for parallelization. Since its field of applications is so broad, the mortar FEM has undergone serious mathematical investigation over the years and has therefore solid theoretical foundations.
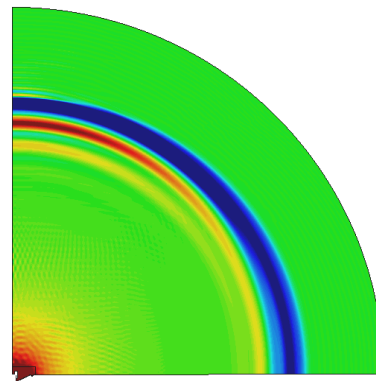
Our next steps in research will be the integration of the mortar FEM with higher order FEM as well as the evaluation for practical applicability of the method to sensor and actuator design.Especially the investigation of the mortar FEM for nonlinear couplings will play a major role in the future.

6   Acknowledgments

References

[1] Mark Ainsworth. Discrete dispersion relation for hp-version finite element approximation at high wave number. *SIAM J. Numer. Anal.*, 42(2):553–575, 2004.

[2] Nina N. Dokeva. *Scalable Mortar Methods for Elliptic Problems on Many Subregions.* PhD thesis, University of Southern California, 2006.

[3] Bernd Flemisch. *Non-matching Triangulations of Curvilinear Interfaces Applied to Electro-Mechanics and Elasto-Acoustics.* PhD thesis, Universität Stuttgart, Institut für Angewandte Analysis und Numerische Simulation, 2006.

[4] Jens Grabinger. Mechanical-acoustic coupling on non-matching finite element grids. Master's thesis, University Erlangen-Nuremberg, June 2007.

[5] M. Kaltenbacher. *Numerical Simulation of Mechatronic Sensors and Actuators.* Springer, Berlin, 2. edition, 2007.

[6] Martin Rausch. *Numerische Analyse und Computeroptimierung von elektrodynamischen Aktoren, am Beispiel eines elektro-dynamischen Lautsprechers.* PhD thesis, Universität Erlangen-Nürnberg, 2001.

[7] Simon Triebenbacher. Nonmatching grids for computational acoustics. Master's thesis, University Erlangen-Nuremberg, January 2006.